TMS alters multivoxel patterns in the absence of overall activity changes

Farshad Rafiei[1], Martin Safrin[2], Martijn E. Wokke[3], Hakwan Lau[4, 5] & Dobromir Rahnev[1]

[1] School of Psychology, Georgia Institute of Technology, Atlanta, GA

[2] School of Medicine, University of California, Los Angeles, Los Angeles, CA

[3] Programs in Psychology and Biology, The graduate Center of the City University of New York, New York

[4] Department of Psychology, University of California, Los Angeles, Los Angeles, CA

[5] The Brain Research Institute, University of California, Los Angeles, Los Angeles, CA

Keywords: Concurrent TMS-fMRI, TMS, PFC, MVPA, BOLD

Author contributions

Experiment 1 was designed by F.R. and D.R; data collection and analysis were performed by F.R. in supervision by D.R. Experiment 2 was designed by all authors together; M.S., M.W., and F.R. collected the data; F.R. and M.S. analyzed the data under the supervision of D.R. and H.L. The manuscript was written by F.R. and D.R. All authors approved the final version of the manuscript.

Acknowledgements

This work was funded by a startup grant to D.R. from the Georgia Institute of Technology.

Corresponding author:
Farshad Rafiei
Georgia Institute of Technology
645 Cherry St. NW
Atlanta, GA 30332
E-mail: farshad@gatech.edu

Abstract

Transcranial magnetic stimulation (TMS) has become one of the major tools for establishing the causal role of specific brain regions in perceptual, motor, and cognitive processes. Nevertheless, a persistent limitation of the technique is the lack of clarity regarding its precise effects on neural dynamics. Here, we examined the effects of TMS intensity and frequency on concurrently recorded blood-oxygen level-dependent (BOLD) signals at the site of stimulation in dorsolateral prefrontal cortex. In Experiment 1, we delivered a series of pulses at high (100% of motor threshold) or low (50% of motor threshold) intensity, whereas in Experiment 2, we always used high intensity but delivered stimulation at four different frequencies (5, 8.33, 12.5, and 25 Hz). We found that the TMS intensity and frequency could be reliably decoded using multivariate analysis techniques even though TMS had no effect on overall BOLD activity at the site of stimulation in either experiment. These results provide important insight into the mechanisms through which TMS influences neural activity.

Introduction

Transcranial magnetic stimulation (TMS) is one of the major tools commonly used both in clinical interventions for diseases, such as depression, and in basic research on the function of different brain areas. However, although much progress has been made (Pasley et al., 2009; Li et al., 2017; Romero et al., 2019a), the precise effects of TMS on neural dynamics remain poorly understood thus limiting progress in clinical as well as basic research applications. One promising technique that can reveal both the local and distant effects of TMS is the application of TMS inside an MRI scanner while concurrently collecting functional MRI (fMRI) data (for recent reviews, see Bestmann and Feredoes, 2013; Bergmann et al., 2016; Polanía et al., 2018).

The feasibility of combining TMS with fMRI was first shown more than 20 years ago (Bohning et al., 1997) and the technique of concurrent TMS-fMRI has further gained in popularity since then (Bestmann and Feredoes, 2013; Heinen et al., 2014a; Leitão et al., 2015; Hawco et al., 2018; Vink et al., 2018a). Most of the initial studies using concurrent TMS-fMRI examined the effects of TMS delivered to the primary motor cortex (M1). This choice was partially driven by the fact that localization of M1 is straightforward and can be ascertained by observing contralateral hand muscle twitches. One ubiquitous finding from these studies is that TMS induces increased blood-oxygen level-dependent (BOLD) activity in the vicinity of the coil for suprathreshold (Bohning et al., 1999; Baudewig et al., 2001; Bestmann et al., 2004) but not subthreshold stimulation intensities (Bohning et al., 2000b; Baudewig et al., 2001; Bestmann et al., 2003, 2004, 2005; Li et al., 2004b; Denslow et al., 2005b). These findings led researchers to conclude that the activation produced by suprathreshold intensities is likely the result of afferent

feedback arising from the induced twitches (Baudewig et al., 2001; Bestmann et al., 2003, 2006; Bestmann and Feredoes, 2013). Similar results have been found when delivering TMS over visual cortex. Specifically, activity under the coil is observed only for intensities high enough to produce phosphene perception (Caparelli et al., 2010), thus suggesting that the observed BOLD activity might be the result of feedback from higher cortical regions responsible for the conscious experience of the phosphenes. These studies highlight the difficulties in characterizing local TMS effects on neural activity independent of their downstream consequences (e.g., twitches or phosphene perception).

Therefore, understanding the local effects of TMS independent of downstream influences arguably requires that TMS is applied outside of the motor and visual cortices. Several studies have targeted areas in the association cortex but were typically not designed specifically to investigate whether TMS produces activations under the coil. Consequently, the results of these studies were inconsistent: some studies reported that in the absence of an explicit task, TMS produces positive BOLD activations in the regions immediately under the coil (Nahas et al., 2001; Li et al., 2004a; Bestmann et al., 2005; Vink et al., 2018b) but many other studies failed to find such activations (Baudewig et al., 2001; Kemna and Gembris, 2003; Li et al., 2004b; Sack et al., 2007; De Weijer et al., 2014; Hawco et al., 2017; Dowdle et al., 2018). These inconsistent results are likely due to the limitations present in many of these studies. Specifically, the majority of studies did not precisely localize the actual location of stimulation and therefore it is unclear whether the reported activations were truly underneath the coil or in nearby regions. Further, some of these studies did not include control conditions and often delivered too few

pulses. These limitations increase the chance of observing both false positives and false negatives. Taken together, it remains unclear whether TMS produces activations under the coil when regions outside of the motor and visual cortices are targeted.

Here we investigated the effect of TMS on brain areas under the coil when applied to the dorsolateral prefrontal cortex (DLPFC) while avoiding the above limitations by precisely localizing the stimulated site, including different control conditions, and delivering a large number of pulses. DLPFC was chosen because it is easily accessible inside the MRI scanner and stimulating it does not result in any motor or visual responses. In Experiment 1, we compared the activations produced by 10 low-intensity pulses delivered at 1 Hz, 10 high-intensity pulses delivered at 1 Hz, and 20 high-intensity pulses delivered in bursts of 4 pulses at 0.5 Hz. In Experiment 2, we compared the activations produced by trains of 30 pulses delivered at four different frequencies (5, 8.33, 12.5, and 25 Hz). Despite the large number of pulses delivered in both experiments, we found no evidence that TMS increased BOLD activity in the brain regions directly under the coil. However, we were able to decode both the intensity (Experiment 1) and frequency (Experiment 2) of stimulation using multivoxel pattern analysis (MVPA). These results demonstrate that different TMS stimulation protocols produce different patterns of activity in the underlying areas in the absence of an overall increase in BOLD activity.

Methods

Subjects

Five subjects (2 females, age range = 24-33) took part in Experiment 1 and six subjects (3 females, age range = 24-37) took part in Experiment 2. Three subjects participated in both of the experiments. Unlike many cognitive studies that seek to aggregate data across subjects, here we were interested in the effects at the level of each individual subject. Therefore, as is common in this type of research (e.g., Rahnev et al., 2013; Huth et al., 2016), we collected data from fewer subjects but tested them extensively. All subjects were medically and neurologically healthy with no history of brain injury, loss of consciousness, or psychiatric diseases. They were all screened for MRI and TMS exclusion criteria and signed an informed consent document. All procedures were approved by the Georgia Tech Institutional Review Board.

Procedures

Experiment 1

In order to determine the effects of TMS under the coil, we employed three different TMS conditions (**Figure 1A**). The first condition consisted of 10 low-intensity (50% of motor threshold) TMS pulses given at a rate of 1 Hz. The second condition consisted of 10 high-intensity (100% of motor threshold) TMS pulses given at a rate of 1 Hz. Finally, the third condition consisted of five bursts of four high-intensity (100% of motor threshold) TMS pulses with individual pulses in a single burst delivered at 12.5 Hz (i.e., there was 80 ms between two consecutive pulses) and individual bursts delivered at 0.5 Hz (i.e., consecutive bursts started 2 seconds apart). These conditions were created so that each lasted 10 seconds. We call the 10-

second period of TMS presentation a "trial." Each trial thus consisted of 10 TMS pulses for Conditions 1 and 2, and 20 TMS pulses for Condition 3. Subjects completed three runs where these three conditions were interleaved, and 10-second breaks were given after every TMS trial. Each run was organized in 10 blocks with each block consisting of three trials (one from each condition in a randomized order). Overall, each run consisted of 30 trials and the whole stimulation period lasted for 600 seconds (10 blocks x 60 seconds per block). We acquired an additional 10 seconds of scanning at the beginning and 5 second of scanning at the end of each run, making each TMS block last a total of 615 seconds. Each run involved the delivery of 400 TMS pulses for a total of 1,200 TMS pulses over the course of the experiment. Throughout the experiment, subjects were asked to fixate on a white fixation cross presented on a gray screen.

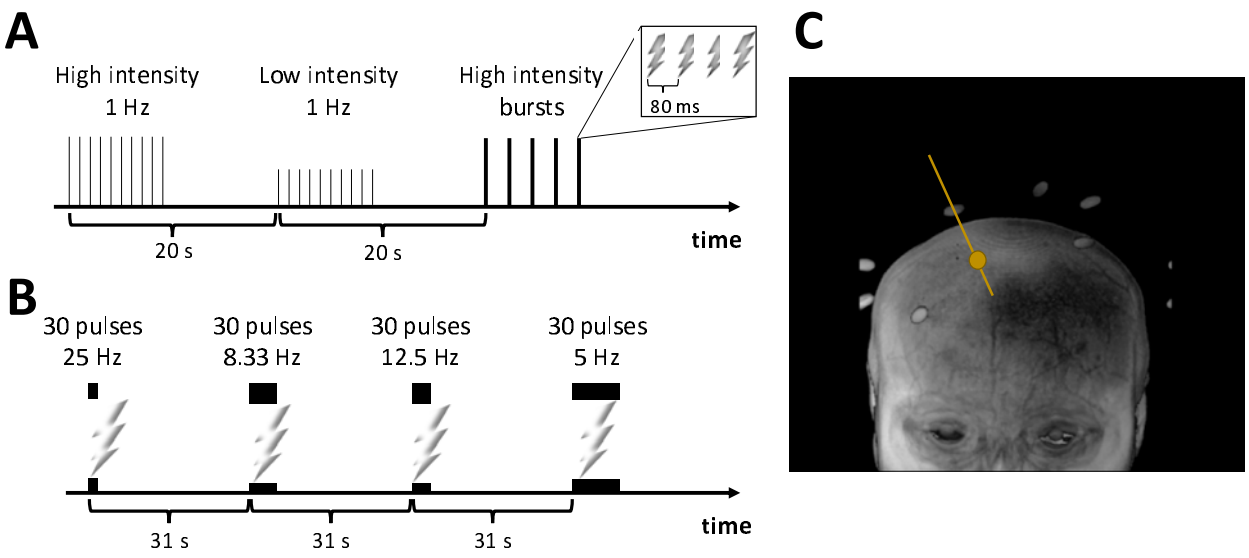

Figure 1. TMS delivery in Experiments 1 and 2. (A) Three conditions were interleaved in Experiment 1: Low intensity 1 Hz, High intensity 1 Hz, and High intensity bursts. Each burst in the High intensity bursts condition consisted of 4 pulses with 80 ms between pulses (see inset). Both 1 Hz conditions delivered 10 pulses with 1 second between consecutive pulses, whereas the High intensity bursts condition consisted of 5 bursts (with 2 seconds between consecutive bursts). The vertical lines indicate individual TMS pulses and their height indicates intensity. (B)

Four conditions were interleaved in Experiment 2: 5, 8.33, 12.5, and 25 Hz stimulation. One trial from each condition consisted of 30 pulses and the onset asynchrony between consecutive trials was 31 seconds. The black boxes indicate the period of stimulation for each trial. (C) Estimation of the stimulation spot. The image shows the anatomical image for one subject. The bright points outside of the brain are the Vitamin E capsules attached to TMS coil. The orange line is the estimated direction of TMS pulses based on the locations of the Vitamin E capsules and the orange circle indicates the stimulation spot located on the brain.

In addition to the TMS scans, we collected two anatomical images, a finger tapping run, and a resting state run. The anatomical images were acquired both in the beginning and at the end of the session to ensure that subject movement did not result in substantial change in the TMS coil position during the experiment. The data from the resting state scan were not analyzed for the purposes of the current paper. The finger tapping run was intended as a control task that can be used to evaluate the power of our setup to detect brain activations, as done in previous concurrent TMS-fMRI studies (Bestmann et al., 2003, 2005; Navarro de Lara et al., 2017a; Vink et al., 2018b). During that run subjects were asked to tap with their right index finger once every second for 10 seconds, followed by a 10-second break with no finger movement. The cue for finger tapping was the fixation cross changing color from black to white. The finger-tapping task thus had the exact same parameters as Conditions 1 and 2 of the TMS run. The finger-tapping run consisted of 15 alterations of finger tapping and rest (as well as a 10-second additional rest at the end of the run) for a total of 310 seconds.

Experiment 2

Experiment 1 included a large number of trials with each trial consisting of more TMS pulses than most previous studies. However, to increase power even more, in Experiment 2 we included two testing sessions and increased the number of pulses per trial even further. The

two sessions were collected on different days separated by less than one week with each session consisting of three TMS runs. We interleaved four different conditions that differed in the frequency of stimulation. In each condition, 30 TMS pulses were given at a rate of 5, 8.33, 12.5, or 25 Hz, respectively. These frequencies were chosen based on the time it takes to acquire a single fMRI slice, which in our protocol was 40 ms (see below). We delivered each TMS pulse so that a single slice would be affected. The four different conditions delivered TMS pulses every 1, 2, 3, or 5 slices thus resulting in frequencies of 25, 12.5, 8.33, and 5 Hz, respectively. The TMS intensity was set to 100% of motor threshold for all conditions. Each run was organized in 5 blocks, each consisting of four trials (one from each condition in a randomized order). We set the distance between the onsets of consecutive trials to 31 seconds (that is, exactly 25 fMRI volumes). Each run thus lasted 682 seconds. Each session consisted of anatomical image acquisition (both at the beginning and end of each session) and three TMS runs.

TMS delivery and timing

TMS was delivered with a magnetic stimulator (MagPro R100, MagVenture), using an MRI-compatible figure of eight coil (MRI-B90). We determined the resting motor threshold (RMT), immediately prior to starting the main experiment as in our previous work (Rahnev et al., 2016; Shekhar and Rahnev, 2018; Bang et al., 2019). We first localized the motor cortex by applying supra-threshold single pulses and determined the location of the right motor cortex as the region that induced maximal twitches of the fingers in the left hand. The resting motor threshold (RMT) was then identified as the intensity which leads to contralateral muscle

twitches on 5 out of 10 trials. The average RMT was 59.20 (SD = 10.06) in Experiment 1 and 60.67 (SD = 2.42) in Experiment 2.

When delivering TMS during fMRI, it is important to ensure that the fMRI data are not compromised. Each TMS pulse only lasts a fraction of a millisecond (about 200 µs) but in some cases it can cause artifacts that last many hundreds of milliseconds or even several seconds. This usually happens when the TMS pulse coincides with the radio frequency (RF) pulse that occurs in the beginning of each fMRI slice. Therefore, it is critical that the TMS pulses are timed so that they do not coincide with RF pulse for any slice. To ensure that our setup avoids such incidences from occurring, we tested our setup using a phantom prior any data collection. We systematically varied the timing of the TMS pulse relative to the beginning of a slice and determined at what delay after the onset of a slice should a TMS pulse be delivered to never result in artifacts that extend beyond the targeted slice. This procedure allowed us to avoid interfering with RF pulse of individual slices and assured to only contaminate a single slice, which significantly simplifies data cleanup (see MRI preprocessing below).

Nevertheless, our procedure still resulted in each TMS pulse creating a large artifact in a single slice. To minimize the data loss, in Experiment 1, we delivered the TMS pulses during slices that would have as minimal as possible of an effect on later analyses. Specifically, in Conditions 1 and 2, which consisted of trains of single pulses at 1 Hz, we delivered the TMS pulse during the acquisition of the lowest brain slice (25th slice in our descending sequence). Similarly, in Condition 3, which consisted of burst of 4 pulses at 80 Hz spaced out by 2 seconds, we

delivered the TMS pulses when acquiring 19th, 21st, 23rd and 25th slices of the brain. We note that these deep slices were never used in the current analyses, so the artifacts created there did not affect our results in Experiment 1. However, such a scheme was not possible in Experiment 2 where 30 slices were delivered in close temporal succession. Instead, to facilitate data cleanup, in Experiment 2 we ensured that a particular slice was never targeted in two consecutive fMRI volumes. This was achieved by making each fMRI volume with 31 slices and starting the sequence in all conditions from slice 1. Thus the 25 Hz condition targeted slices 1, 2, …, 30 from a single volume, the 12.5 Hz condition targeted slices 1, 3, 5, …, 31 in the first volume and slices 2, 4, 6, …, 28 in the second volume, etc.

TMS targeting

In Experiment 1, we targeted left DLPFC by placing the TMS coil over the left dorsal frontal region of an individuals' brain. In Experiment 2, we targeted a site in left DLPFC that had been identified for each individual subject from a previous scan. Specifically, the stimulation site was defined as a region in the left middle frontal gyrus with largest negative connectivity with the subgenual nucleus. We marked this region in subjects' anatomical space and used the titanium-based, MRI-compatible Localite TMS Navigator and camera stand to position the coil over the identified location. In both experiments, we ensured that our TMS site did not result in any muscle twitches by first delivering several TMS pulses immediately after positioning the coil and closely monitoring the subject's contralateral part of the body.

Regardless of the targeting method used, we wanted to independently verify the exact location of stimulation in both experiments. Therefore, we designed a procedure where we attached seven Vitamin E capsules on the surface of the TMS coil in order to help us determine the exact placement of the coil. Six of the Vitamin E capsules were placed on the bottom surface of the coil in a hexagon shape centered on the middle of the TMS coil. Averaging the location of all six Vitamin E capsules gave us the center of the hexagon, which allows us to determine the exact location of the center of the TMS coil. To determine the exact axis of stimulation, we used the last Vitamin E capsule, which was attached at the center of the coil but on its upper surface. The axis of stimulation (or entry line) was then computed by finding the equation of a line which passes through the seventh Vitamin E capsule and is perpendicular to the plane created by the first six capsules.

The procedure additionally allowed us to estimate how much the location of entry into the brain shifted over the course of each experiment. To do so, we coregistered the anatomical images collected at the beginning and end of each session determined the stimulation spot separately for each of them. Finally, we calculated the coil displacement over the course of the experiment as the distance between these two points.

MRI data acquisition

Data collection was performed on a Siemens 3T Trio scanner. Since the TMS coil is too large to fit into standard MRI coils, we employed a setup that consists of the bottom part of a 12-channel coil together with a 4-channel FLEX coil that wraps on the top of the subject. This setup

allowed us to obtain full brain coverage with very high SNR in comparison to conventional setups consisting of either a single-channel birdcage coil or a dedicated coil which does not provide whole brain coverage (Triantafyllou et al., 2011; Navarro de Lara et al., 2017b; Wang et al., 2017). High resolution T1-weighted anatomical images were acquired with MPRAGE pulse sequence (FoV = 256 mm; TR = 2250 ms; TE = 3.98 ms; 176 slices; flip angle = 9˚; voxel size = 1.0 × 1.0 × 1.0 mm^3). Functional images were acquired using a T2*-weighted gradient echo-planar imaging sequence. In order to increase our signal near the site of stimulation, in Experiment 1 we used a TR of 1,000 ms and 25 descending slices (40 ms per slice) positioned near the top of head. On the other hand, Experiment 2 aimed for a full-brain coverage and used TR of 1,240 ms and 31 descending slices (40 ms per slice). All other parameters were equivalent between the two experiments (FoV = 220 mm; TE = 30 ms; flip angle = 50˚; voxel size = 3.0 × 3.0 × 3.5 mm^3).

MRI preprocessing

All analysis steps were performed in SPM12. We first transformed the original DICOM images to NIFTI format and removed all TMS-related artifacts in the following manner. In Experiment 1, since the deepest slice of the brain (25th slice) was contaminated in all stimulation conditions, we removed this slice from further analysis in the whole dataset for all subjects. In addition, for Condition 3 of Experiment 1 and for all conditions of Experiment 2, we removed each targeted slice and substituted it with the first order interpolation (i.e., mean) of the same slice number from the previous and next volumes. Finally, to ensure that the data were free from any additional signal loss, we checked for artifacts in every single slice by examining the average signal amplitude in each slice over the time course of each run of both experiments. Deviations

of more than four standard deviations were flagged as outliers (less than 0.05% in Experiment 1 and less than 0.5% in Experiment 2) and removed by a first order interpolation of the same slice number from the previous and next volumes. If any of the slices used in the interpolation were also flagged as outliers, we removed both slices and used a first order interpolation of the closest slices not flagged as outlier.

After removing the TMS-related artifacts, we implemented standard preprocessing. We first performed additional despiking using the 3dDespike function in AFNI. The fMRI images were then slice-time corrected, realigned to the first volume of the run, coregistered to the anatomical image acquired at the beginning of the session (reference image), normalized to MNI anatomical standard space and spatially smoothed with a 6 mm full width half maximum (FWHM) Gaussian kernel. The same preprocessing steps, except for the TMS artifact removal, were also performed for the finger tapping run in Experiment 1.

GLM analyses

In both experiments, we constructed a general linear model (GLM). In Experiment 1, the GLM consisted of 10 regressors for each run. The first three regressors modeled the blood-oxygen level-dependent (BOLD) responses related to each 10-second TMS trial for Condition 1 (Low intensity single pulse), Condition 2 (High intensity single pulse), and Condition 3 (high intensity burst of pulses). In Experiment 2, the GLM consisted of 11 regressors for each run. The first four regressors modeled the BOLD responses related to each TMS trial of the four TMS conditions. We included six regressors related to head movement (three translation and three rotation

regressors) and a constant term. In all cases, the BOLD response was modeled with canonical hemodynamic response function (HRF). The activation maps for each subject were obtained by applying t-test to the GLM parameter estimates obtained for each condition.

To further explore the effect of TMS specifically on the area immediately under the coil with higher statistical power, we defined spherical regions of interest (ROIs) underneath the TMS coil with radii of 8, 12, 16, and 20 mm using MarsBar (Brett et al., 2002). The centers of these spheres were placed on the TMS entry line and were set so that the entire ROI fell inside the brain. The same GLMs defined above were used to estimate the beta values for each condition in every ROI in both experiments.

MVPA

In addition to the GLM analyses, we performed multi-voxel pattern analyses (MVPA) within the spherical ROIs defined under the coil. The MVPA analyses were performed on the beta values in each voxel derived from the GLM created for univariate analysis purposes. In Experiment 1, we had a total of 90 events (3 conditions x 30 events per condition). We used support vector machine classification with leave-one-run-out (3-fold) scheme implemented by The Decoding Toolbox (TDT) (Hebart et al., 2015). For each classification fold, beta estimates for each condition for two runs were used as training data, and the performance was tested on data from the third ('left-out') run. This was performed iteratively until all runs had been tested (i.e., 3 iterations total). The accuracy of the classifier was computed separately for each ROI and each subject by averaging the classification accuracy over all folds. We followed a similar

procedure for the analyses in Experiment 2 and applied a Gaussian Naïve Bayes (GNB) classifier to each session separately. We used TDT toolbox to generate the feature vectors and performed the analysis in the Waikato Environment for Knowledge analysis (WEKA) software (Frank et al., 2016). We further examined whether a classifier trained on one pair of frequencies can be used to classify a different pair of frequencies. Specifically, we trained a classifier to distinguish between 5 and 25 Hz TMS using the voxels in 20-mm ROI and examined the ability of this classifier to distinguish between 8.33 and 12.5 Hz TMS.

In a separate analysis we explored whether the voxels that were most informative for classification were located near the TMS coil. We performed dimensionality reduction on the 20-mm ROI in order to identify the most informative voxels (i.e., the voxels with the most information with respect to classes; average number of selected voxels = 83.75 voxels, SD = 8.76 voxels). We employed information gain dimensionality reduction based on Gini impurity index (Langs et al., 2011). Given the rapid decrease of the magnetic field away from the TMS coil, we hypothesized that the informative voxels should fall mostly in upper hemisphere of the ROI. One potential concern with this analysis is that the upper hemisphere may contain more gray matter voxels, thus making any comparisons trivial. To check whether this was indeed the case, we determined the number of grey matter voxels in upper and lower hemispheres and ensured that these numbers did not differ.

Statistical analyses were performed by fitting mixed models using the Nonlinear Mixed-Effects Models (*nlme*) library (Pinheiro et al., 2019) in R (R Core Team (2019). R: A language and environment for statistical computing. R Foundation for Statistical Computing, Vienna, Austria.

URL https://www.R-project.org/.) The models were fit to the accuracy of the classification for each trial or to the proportion of gray matter voxels in the upper hemisphere of the 20-mm ROI for each subject. In the analyses for Experiment 1, subject was defined as a random effect. In the analyses for Experiment 2, both subject and session were defined as random effects. In all cases, the intercept was compared to chance level.

Data and code

Processed data including beta values and classification for each subject and easy ROI, as well as codes for analyzing these data are freely available at osf.io/z5jtg.

Results

We investigated the effect of TMS on BOLD activity under the coil when targeting DLPFC using a novel concurrent TMS-fMRI setup. In Experiment 1, we employed three types of TMS protocols that differed in both intensity (50% vs. 100% of motor threshold) and frequency of stimulation (**Figure 1A**). In Experiment 2, we only used high intensity (100% of motor threshold) pulses but systematically varied the stimulation frequency (5, 8.33, 12.5, and 25 Hz). To understand the effects of TMS, we performed conventional univariate analyses, as well as multivariate decoding.

Experiment 1

Setup validation

We employed a novel concurrent TMS-fMRI setup in which MRI images were collected using a combination of the bottom half of a standard 12-channel coil together with a 4-channel FLEX coil positioned over subjects' forehead. Pilot data suggested that this setup produces higher temporal signal-to-noise ratio (tSNR) than conventional birdcage coils while allowing for full-brain coverage unlike newer setups (Navarro De Lara et al., 2015; Navarro de Lara et al., 2017b). Nevertheless, we wanted to confirm that our new setup can detect changes in the BOLD signal in a task designed to have a similar structure as our TMS protocol. We therefore employed a finger tapping task that has previously been used in concurrent TMS-fMRI studies as a point of reference for the effects of TMS applied to M1 (Boecker et al., 1994; Baudewig et al., 2001; Bestmann et al., 2003; Dechent and Frahm, 2003). Subjects pressed a button box using their right index finger whenever a visual cue was presented on the screen with the

presentation of the visual cue being identical to the 1 Hz TMS stimulation conditions such that 10 cues presented at 1 Hz alternated with 10-second blocks of rest.

Despite the fact that the finger tapping task was substantially shorter than the TMS task (5 minutes vs. 30 minutes total), we found that, compared to periods of rest, periods of finger tapping produced significant BOLD signal increase (at $p < .05$ FWE) in left M1 and supplementary motor area (SMA) for all subjects (**Figure 2**). These activations are in line with previously reported activity patterns evoked by the finger tapping task (Boecker et al., 1994; Baudewig et al., 2001; Bestmann et al., 2003; Dechent and Frahm, 2003). These results establish that our novel setup allows us to robustly detect cortical activations in dorsal regions of the brain thus demonstrating that it can be used to detect TMS-related activations in nearby brain regions.

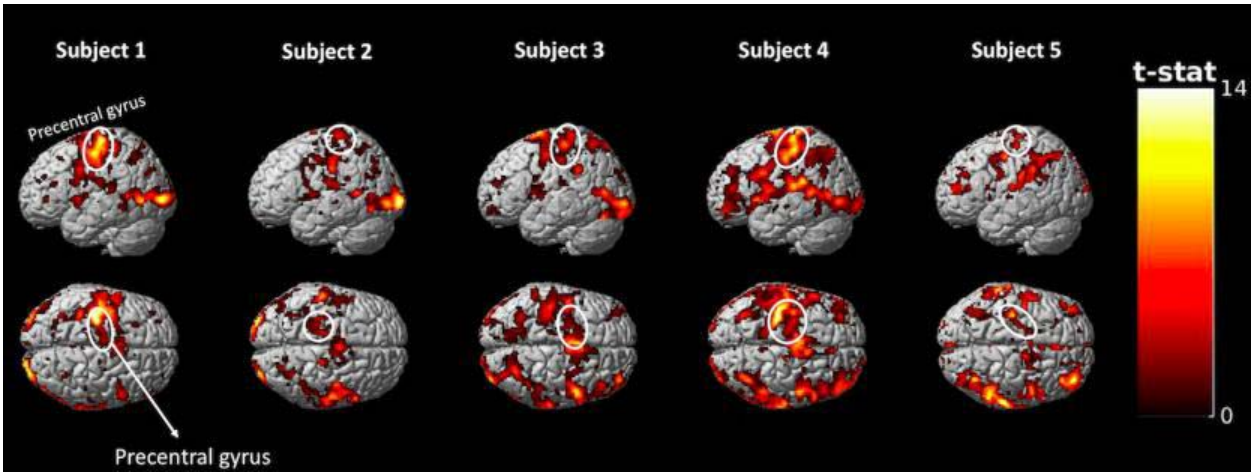

Figure 2. Activation maps obtained from a 5-minute finger tapping task. The finger tapping task produced robust activations in both the primary motor cortex (M1) and supplementary motor area (SMA) for each one of the five subjects. These results demonstrate the ability of our novel concurrent TMS-fMRI setup to detect activity in the dorsal surface of the brain. For

display purposes, the activation maps are generated using $p < .001$, uncorrected. Colors indicate t-values.

Further, we checked whether the position of the TMS coil remained stable over the course of the experiment. We found that the average displacement across subjects was 2.32 mm (range: 1.9 - 2.8 mm). Therefore, the coil position remained fairly stable over the course of the experiment and moved less than the length of a single voxel.

TMS to DLPFC produces no activation under the coil

Having validated our setup, we turned our attention to the question of whether TMS to DLPFC produces BOLD activity under the coil. To explore specifically the direct neural effects of TMS, we generated a contrast for High intensity 1 Hz > Low intensity 1 Hz, as well as a contrast for High intensity bursts > Low intensity 1 Hz. We used low intensity stimulation as control to account for the indirect effects of TMS such as auditory and tactile sensations associated with the stimulation. We found that both comparisons failed to show a clear increase in activity under the coil for high > low intensity TMS even at the liberal threshold of $p < .001$ uncorrected (**Figure 3**). Specifically, subjects 1 and 2 showed hints of positive and negative activations under the coil, respectively, whereas the rest of the subjects showed no positive or negative activations in the vicinity of the coil.

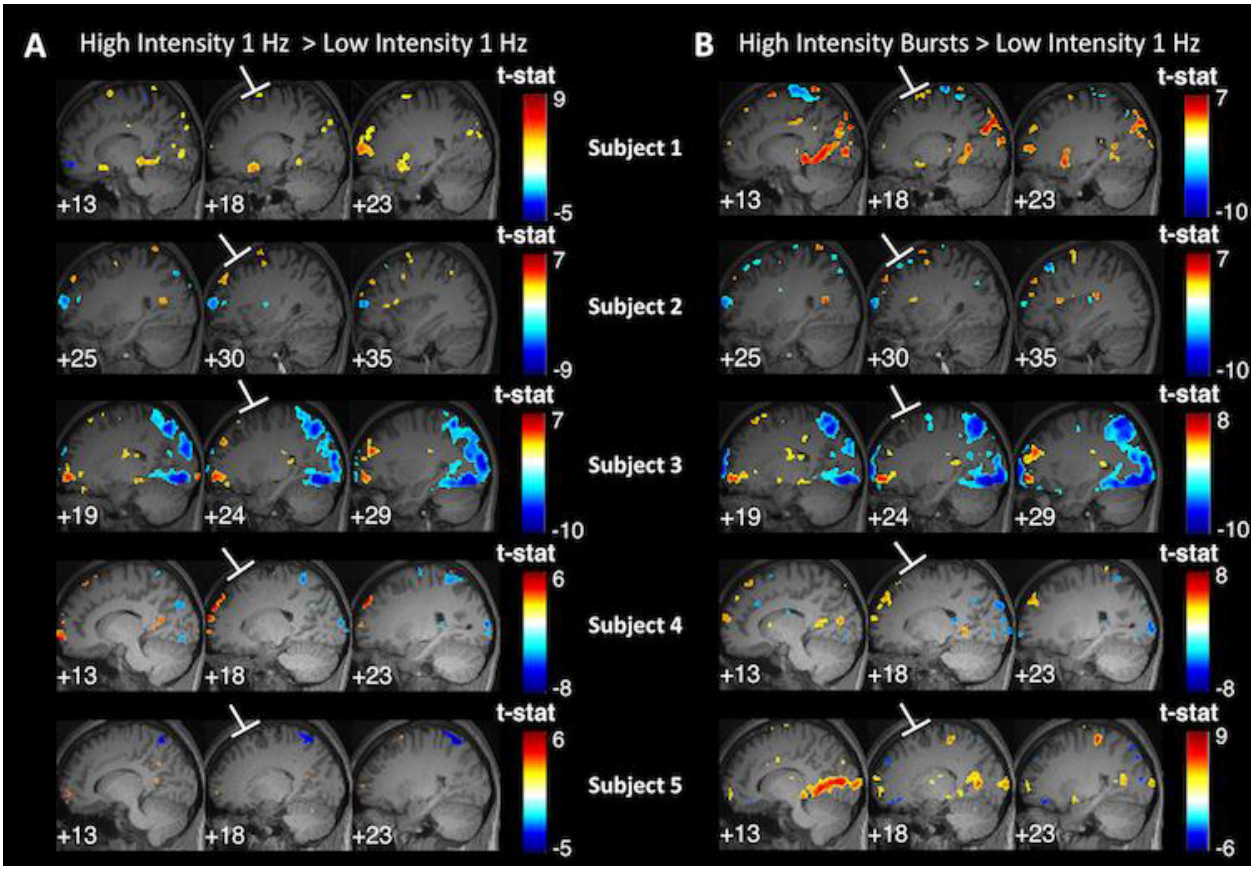

Figure 3. TMS to DLPFC produces no activation under the coil. We contrasted each of the two high-intensity TMS conditions against the low-intensity TMS condition. (A) High intensity 1 Hz > Low intensity 1 Hz contrast. (B) High intensity bursts > Low intensity 1 Hz contrast. For both panels, sagittal slices are centered at the site of stimulation (middle column), as well as on the slices 5 mm to the left and right (left and right columns). The activation maps show a lack of systematic activation immediately under the coil and suggest the presence of large variability in remote areas across subjects. Activation maps generated using $p < .001$, uncorrected; colors indicate t-values.

Nevertheless, it could be argued that $p < .001$, uncorrected is still a fairly conservative threshold, which may mask the existence of small but consistent activations under the coil. Therefore, we examined the same brain activation maps at $p < .05$, uncorrected (**Supplementary Figure 1**) and found that the pattern of results remained the same. To further explore the effect of TMS on the area directly under the coil, we defined spherical ROIs with

radii of 8, 12, 16, and 20 mm and examined the BOLD signal change in these ROIs. We found no consistent pattern of positive or negative activations for any of the contrasts between the three different TMS conditions (**Figure 4**). Specifically, the two contrasts comparing high- to low-intensity TMS ("High intensity 1 Hz > Low intensity 1 Hz" and "High intensity bursts > Low intensity 1 Hz") featured a total of 20 positive and 20 negative contrast estimates. Overall, the parameter estimates were not significantly different from zero for any of the 12 comparisons (3 contrasts X 4 ROI sizes; all *p*'s > .2). Finally, when examining each individual subject separately, we found that a total of three out of the possible 60 comparisons (3 contrasts X 4 ROI sizes X 5 subjects) were significantly higher than zero at the .05 level. This number of significantly positive activations (3/60 = 5% of all comparisons) is similar to what would be expected to happen by chance in the absence of any true differences between the conditions. These results clearly show that there was no reliable difference in the level of BOLD signal change under the coil between the three TMS conditions despite the large differences in stimulation intensity and number of pulses.

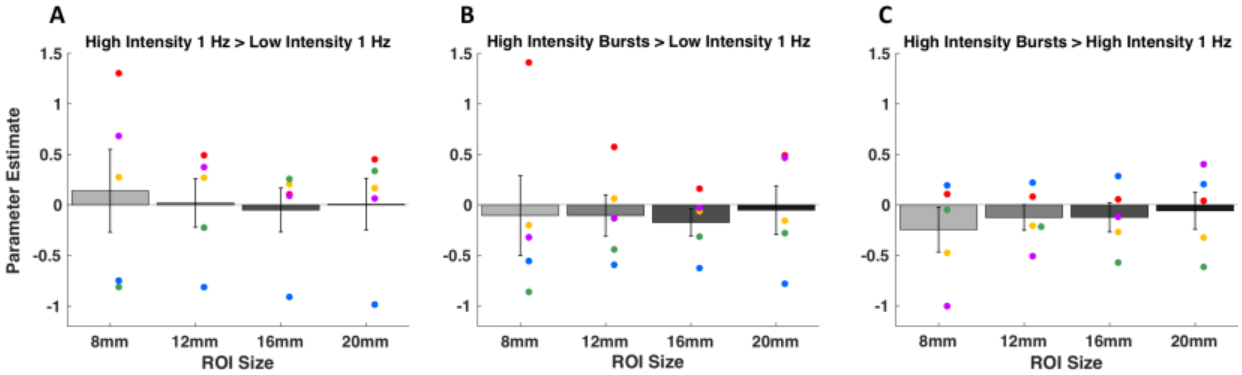

Figure 4. Parameter estimates for the comparisons between the three different TMS conditions in ROIs of different sizes. We plotted the parameter estimates for each contrast in the direction of the expected activations (high minus low intensity and more pulses minus fewer pulses). We further examined ROIs directly under the coil of four different sizes using radii of 8, 12, 16, and 20 mm. (A) High intensity 1 Hz > Low intensity 1 Hz contrast. (B) High intensity bursts > Low intensity 1 Hz contrast. (C) High intensity bursts > High intensity 1 Hz contrast. We found no consistent pattern of positive or negative activations for any of the three contrasts and any of the ROI sizes. Error bars represent SEM, colors represent unique subjects.

TMS condition can be decoded under the coil

The lack of consistent increase of BOLD activity under the TMS coil raises the question of whether any TMS effects under the coil can be detected using fMRI at all. To address this question, we examined the distributed patterns of activity and built an MVPA classifier which attempted to distinguish the different TMS conditions. We built a separate classifier for each of the four ROI sizes (radii of 8, 12, 16, and 20 mm) and used 3-fold cross validation by training the classifier on two TMS runs and testing on the remaining run.

In a first analysis, we performed 3-way classification on the three TMS conditions (Low intensity 1 Hz, High intensity 1 Hz, and High intensity bursts). Across the four ROI sizes, 17 out of the 20 classifications were above the chance level, two were below chance level, and one was exactly at the chance level. To quantify the classification accuracy for each ROI, we performed a mixed model analysis on the individual TMS trials for classification with subject as a random effect and accuracy of classification as the dependent variable. We found that the intercept value indicating the classification accuracy in the group was significantly higher than the intercept expected by chance-level classification for all four ROI sizes (8-mm ROI: $t(445) = 2.03$, $p = .04$; 12-mm ROI: $t(445) = 4.07$, $p = 5 \times 10^{-5}$; 16-mm ROI: $t(445) = 3.03$, $p = .0026$; 20-mm ROI: $t(445) = 4.09$, $p = 5 \times 10^{-5}$; **Figure 5A**). The larger ROI sizes generally produced higher intercepts indicating better classification performance, likely due to the larger number of voxels included. These results indicate that MVPA successfully distinguished the BOLD activity patterns evoked by the different TMS conditions despite the absence of consistent univariate activations.

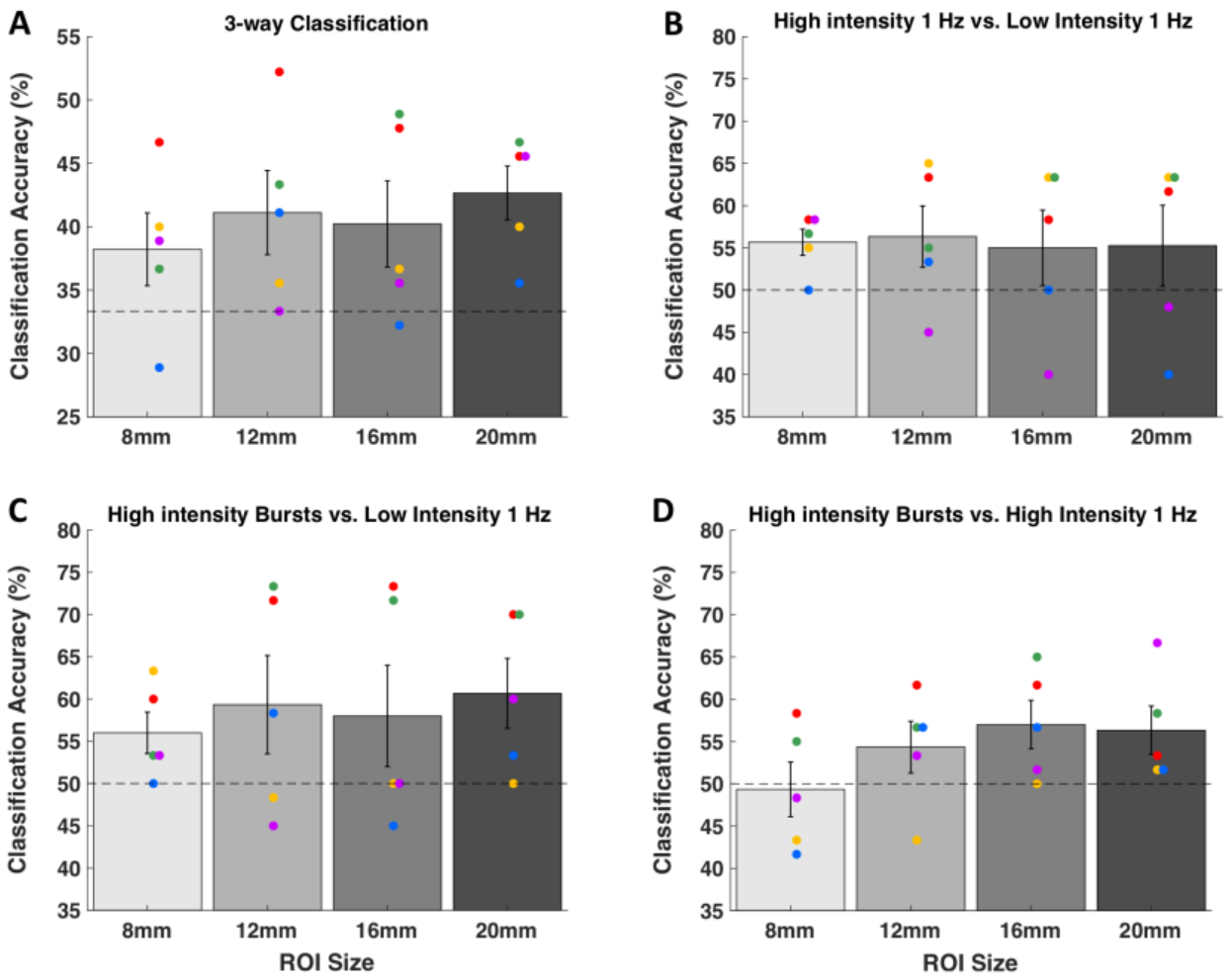

Figure 5. Decoding the TMS condition using MVPA in different ROI sizes under the coil. (A) Three-way classification performance for the different TMS conditions (High intensity bursts, High intensity 1 Hz, and Low intensity 1 Hz). (B-D) Two-way classification performance for each pairwise comparison of different TMS conditions. Dashed lines show chance level (33.33% in Panel A, 50% in Panels B-D). Error bars represent SEM, colors represent unique subjects.

Further, we examined whether the above-chance classification performance in the 3-way classification was due to any specific pair of conditions. To do so, we build additional 2-way MVPA classifiers to distinguish between all pairs of conditions drawn from the three TMS conditions. We first investigated classification performance in the 20-mm ROI since that ROI

provided the best 3-way classification performance. We found that the classification accuracy of the combined data using mixed model analysis was numerically highest when comparing the High intensity bursts vs. Low intensity 1 Hz conditions (accuracy = 60.7%, chance level = 50%, t(295) = 2.87, p = .0042; **Figure 5B**) and slightly lower for the other two comparisons (High intensity bursts vs. High intensity 1 Hz: accuracy = 56.3%, t(295) = 2.21, p = .0280; High intensity 1 Hz vs. Low intensity 1 Hz: accuracy = 55.3%, t(295) = 1.25, p = .2116; **Figure 5C,D**) but the difference in classification accuracy was not significantly different between the three comparisons (all three p's > .1, Z tests for proportions). We found qualitatively similar results for the 16-mm, 12-mm, and 8-mm ROIs (**Figure 5B-D**) with classification generally being above chance but classification accuracy not being significantly different between the three comparisons. These results suggest that the successful 3-way classification was likely not driven by any one particular condition.

Experiment 2

Experiment 1 demonstrated that TMS conditions that vary in the intensity of stimulation and number of pulses delivered do not result in differential activation under the coil but can be successfully distinguished using MVPA. In Experiment 2, we sought to extend these findings by exploring whether the same pattern of results would be obtained when varying TMS frequency while keeping both the intensity of stimulation (100% of motor threshold) and number of pulses (30 per train) the same across conditions. We again targeted DLPFC but used four different frequencies – 5, 8.33, 12.5, and 25 Hz – and analyzed the pattern of activity under the coil by employing both univariate and multivariate techniques. Similar to Experiment 1, we

computed TMS coil displacement from the beginning to the end of the experiment, and found that movement of the coil was relatively small (average = 2.23 mm, range: 1-3.7 mm).

Stimulation frequency does not modulate BOLD activity under the coil

We first compared the BOLD signal change between every two pairs of frequencies. We found no reliable univariate effect: no frequency produced consistently higher activity under the coil compared to any other frequency even at the liberal threshold of $p < .001$ uncorrected (**Figure 6**). Similar to Experiment 1, we observed substantial across-subject variability in the activations induced in remote areas but relatively smaller within-subject variability across the two sessions completed by each subject.

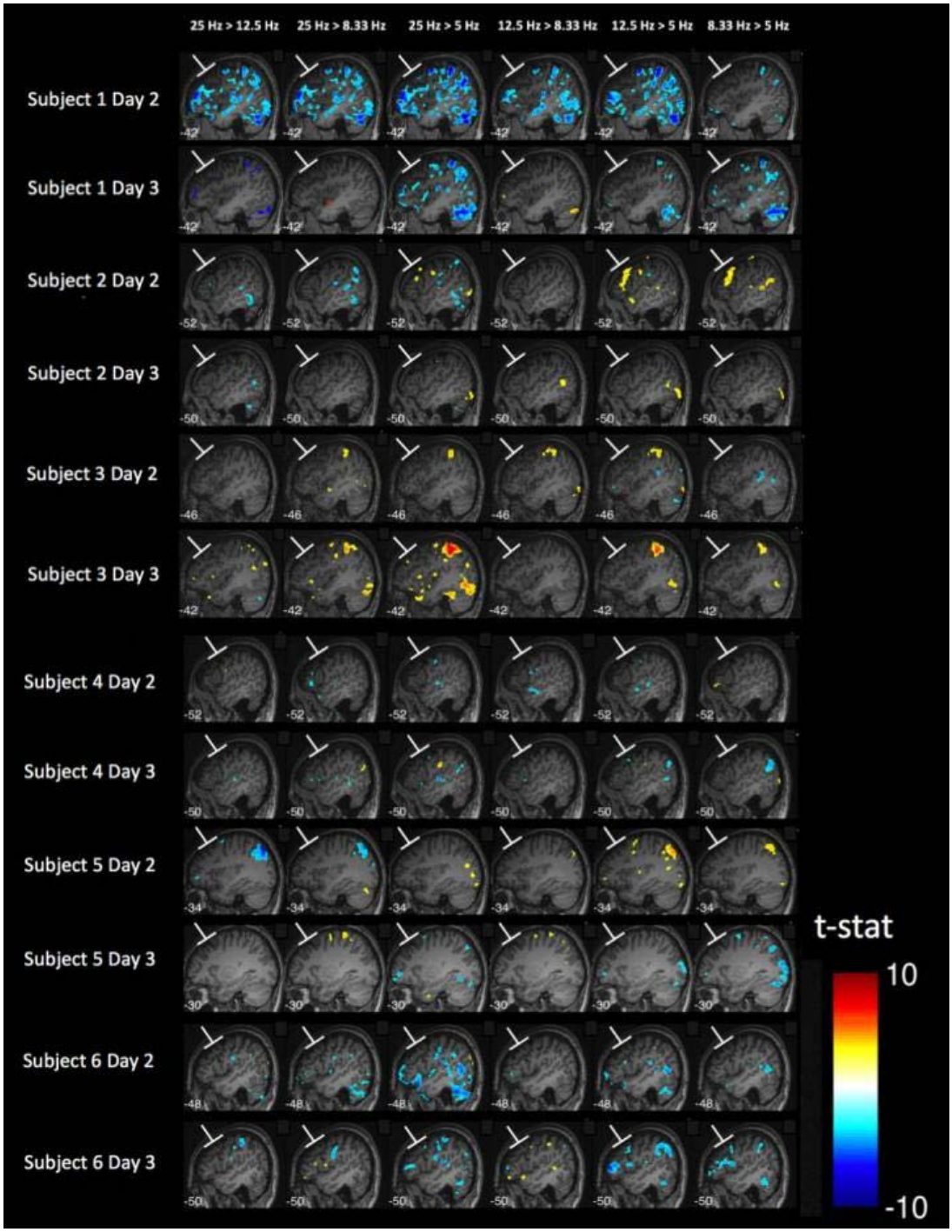

Figure 6. Different TMS frequencies do not produce differential activation under the coil. Sagittal slices of the brain are shown at the location of stimulation spot for each of the six pairwise comparisons between the four different TMS frequencies used in Experiment 2. For each subject, data from the two TMS sessions (Day 2 and Day 3) are shown in separate rows. No frequency resulted in consistently higher activity than any other frequency. Activation maps generated using $p < .001$, uncorrected; colors indicate t-values.

As in Experiment 1, we further explored the activity directly under the coil by examining the BOLD effects in spherical ROIs with radii of 8, 12, 16, and 20 mm. We again found no consistent pattern of positive or negative activations for any of the contrasts between the four different TMS frequencies (**Figure 7**). We performed mixed model analyses on the individual-subject parameter estimates with subject and day of testing as random effects. We found that the intercept for the parameter estimates were not significantly different from zero for any of the 24 comparisons (6 pairs of conditions X 4 ROI sizes; all *p*'s > .05). Finally, when examining each comparison for each individual subject separately, we found that a total of 12 out of the possible 288 comparisons (6 pairs of conditions X 4 ROI sizes X 6 subjects X 2 days) were significantly different than zero at the .05 level (rate of significance = 4.17%, which is similar to the 5% rate that would be expected by chance). These results suggest that the four different TMS frequencies did not result in reliable differences in evoked BOLD activity under the coil.

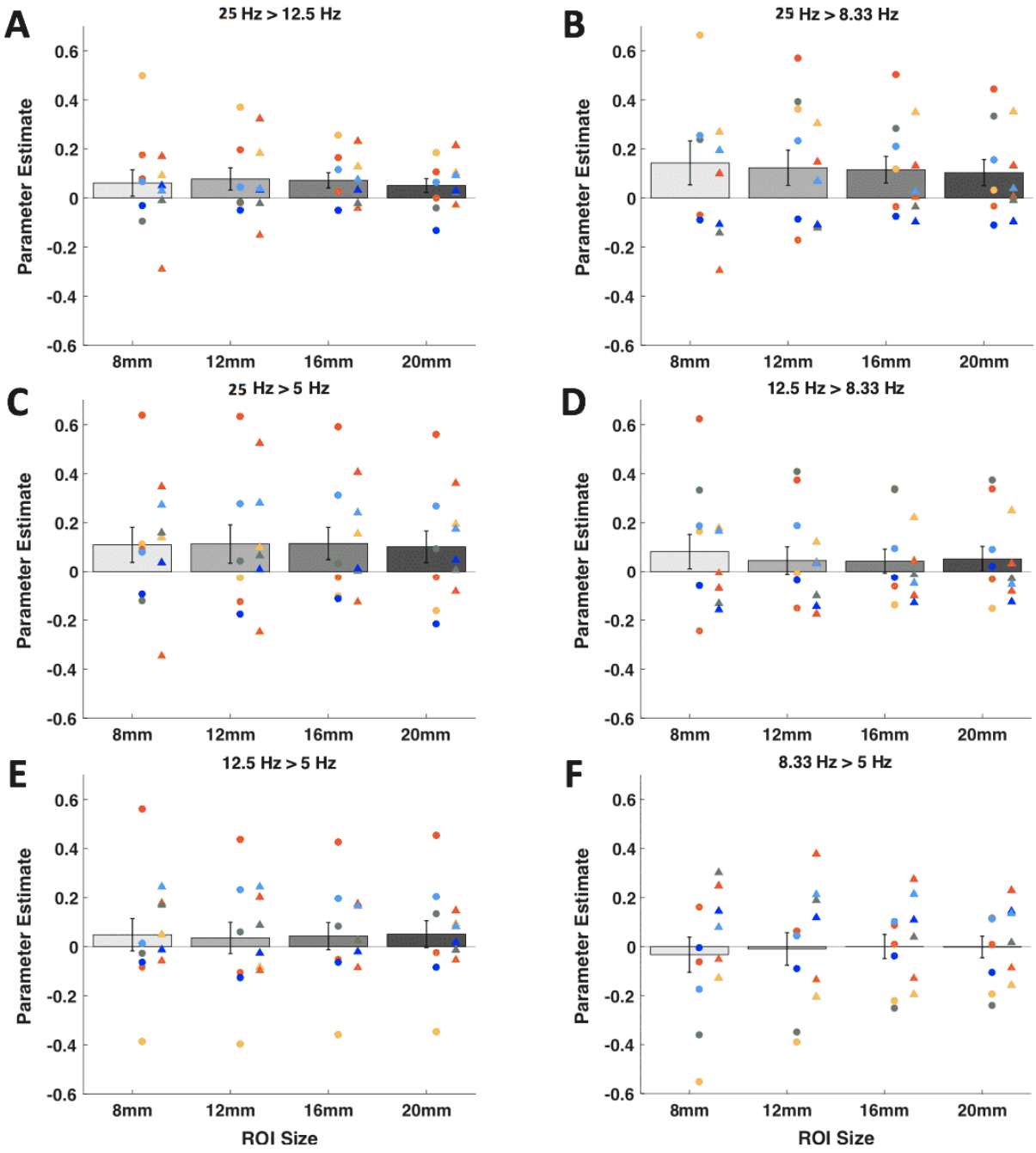

Figure 7. Parameter estimates for the comparisons between the four different TMS frequencies in ROIs of different sizes. We plotted the parameter estimates for higher minus lower TMS frequencies. We further examined ROIs directly under the coil of four different sizes using radii of 8, 12, 16, and 20 mm. (A) 20 Hz > 12.5 Hz contrast. (B) 20 Hz > 8.33 Hz contrast. (C) 20 Hz > 5 Hz contrast. (D) 12.5 Hz > 8.33 Hz contrast. (E) 12.5 Hz > 5 Hz contrast. (F) 8.33 Hz > 5 Hz contrast. We found no consistent pattern of positive or negative activations for any of the six contrasts and any of the ROI sizes. Error bars represent SEM, colors represent unique subjects with data from Day 2 plotted as a circle and data from Day 3 plotted as a diamond.

The frequency of stimulation can be decoded under the coil

Similar to Experiment 1, we examined whether the lack of consistent BOLD activity differences between the four TMS frequencies implies that TMS frequency has no impact on BOLD activity under the coil at all. To address this question, we again built an MVPA classifier to distinguish between the different TMS frequencies. We built a separate classifier for each of the four ROI sizes (radii of 8, 12, 16, and 20 mm). We again used 3-fold cross validation by training on two TMS runs and testing on the remaining run, and performed a 4-way classification on the four frequencies.

Performance of all 48 classifiers (6 subjects X 2 days X 4 ROI sizes) were above chance level. As in Experiment 1, to quantify the classification accuracy for each ROI, we performed mixed model analyses with subject and day of testing as random effects and individual trial accuracy as the dependent variable. We found that the intercept was significantly higher than expected by chance for all ROI sizes (8-mm ROI: $t(708) = 20.77$, $p = 3.4 \times 10^{-75}$; 12-mm ROI: $t(708) = 24.33$, $p = 1.7 \times 10^{-95}$; 16-mm ROI: $t(708) = 24.54$, $p = 9.8 \times 10^{-97}$; 20-mm ROI: $t(708) = 22.60$, $p = 1.4 \times 10^{-86}$; **Figure 8**). The classification accuracy increased slightly for larger ROI sizes possibly because they contain more voxels compared to smaller ROIs. These results show that, just as in Experiment 1, decoding analyses based on the pattern of BOLD activations across different voxels under the coil successfully distinguished the four different TMS frequencies even in the absence of consistent univariate differences between these frequencies.

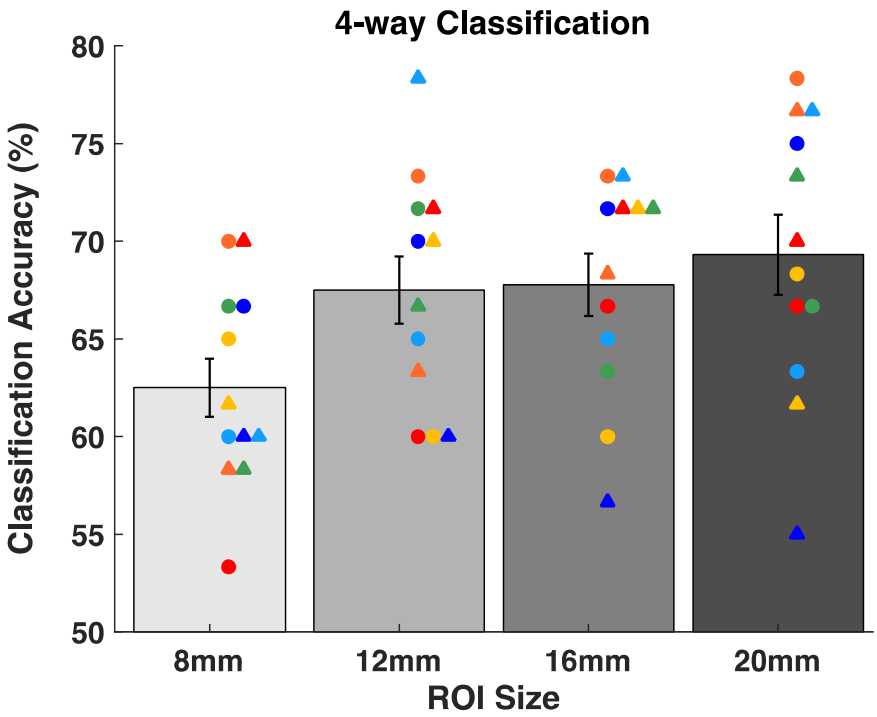

Figure 8. Decoding the TMS frequency using MVPA in different ROI sizes under the coil. Four-way classification performance for the four different TMS frequencies (5, 8.33, 12.5, and 25 Hz). Significant classification accuracy was obtained for all ROI sizes. Error bars represent SEM, colors represent unique subjects with data from Day 2 plotted as circles and data from Day 3 plotted as triangles. Chance classification is 25%.

We further examined the relationship between the different frequencies by testing whether a classifier trained on one pair of frequencies can be used to classify a different pair of frequencies. Specifically, we trained a classifier to distinguish between 5 and 25 Hz TMS using the voxels in the 20-mm ROI. This classifier had very high cross-validation accuracy (mean classification accuracy = 97.50%, t(348) = 57.65, $p = 4.1 \times 10^{-180}$; **Figure 9**) demonstrating that the 5 and 25 Hz conditions resulted in very different patterns of activity despite the fact that neither led to consistently higher activations than the other. Critically, we used this same classifier to discriminate between 8.33 and 12.5 Hz TMS. We found that the classifier trained on

5 vs. 25 Hz stimulation was able to reliably distinguish between 8.33 and 12.5 Hz stimulation (mean classification accuracy = 80.28%, t(348) = 14.42, $p = 2.8 \times 10^{-37}$; **Figure 9**), suggesting that the activation patterns changed monotonically for the four frequencies.

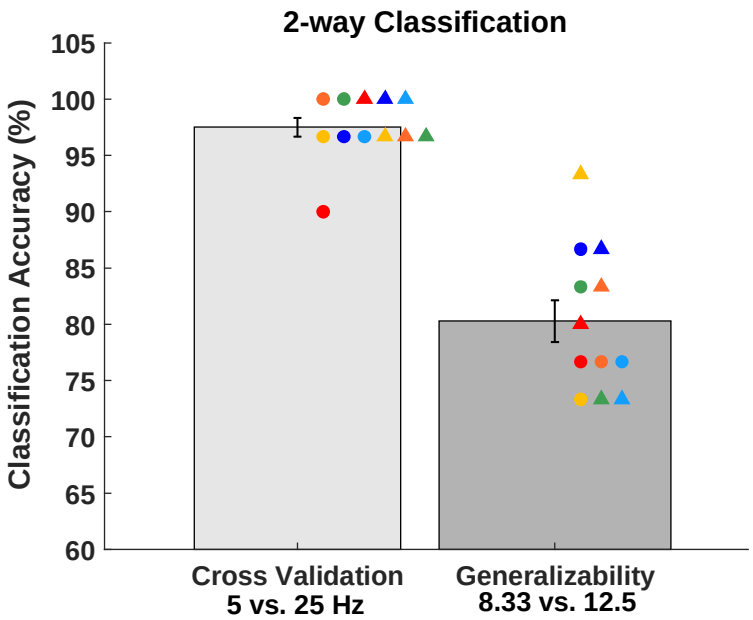

Figure 9. Relationship between the activation patterns of different frequencies. We trained a classifier to distinguish between 5 and 25 Hz stimulation and tested whether it can distinguish between 8.33 and 12.5 Hz stimulation. The classifier had very high cross-validation accuracy for the 5 vs. 25 Hz classification. Critically, it was able to also distinguish between 8.33 and 12.5 Hz stimulation even though it was never trained on these frequencies. Chance level was 50%.

Finally, we examined whether the voxels that were most informative for classification were located near the TMS coil. Given the rapid decrease of the magnetic field away from the TMS coil, we hypothesized that TMS should have a smaller influence on the voxels in the lower half of the large ROI sizes. To test this hypothesis, we performed dimensionality reduction where we identified the most informative voxels (that is, the voxels with the most information with respect to classes; Langs et al., 2011). We found that the majority (63.92%) of these voxels were

located in the upper half of the 20-mm ROI where the TMS magnetic pulses are the strongest ($t(6) = 4.28$, $p = 0.0052$). This clustering of informative voxels in the upper half of 20-mm ROI occurred despite the fact that the number of gray matter voxels in the upper vs. lower half of the ROI were not significantly different ($t(6) = 0.55$, $p = 0.6022$). These results demonstrate that the voxels closest to the TMS coil carried the most information about classification.

Discussion

We investigated the effect of TMS on BOLD activity and MVPA decodability immediately under the TMS coil. In two experiments, we observed that both the intensity and frequency of stimulation could be reliably decoded directly underneath the TMS coil. On the other hand, TMS had no effect on overall BOLD activity underneath the coil even when bursts of up to 30 high-intensity pulses were employed. These results suggest that the effects of TMS on the underlying neural tissue may be more complex than previously appreciated but that decoding methods are sensitive to variations in both TMS intensity and frequency.

Many previous concurrent TMS-fMRI studies delivered TMS over motor (Bohning et al., 1999, 2000a; Baudewig et al., 2001; Bestmann et al., 2003, 2004; Denslow et al., 2005a) or visual cortex (Caparelli et al., 2010). However, a major difficulty in interpreting the results of these studies is that the observed activations could be a combination of local effects and afferent feedback arising from the induced twitches or visual phosphenes (Bestmann et al., 2008). Therefore, in order to specifically examine the local effects of TMS independent of its downstream consequences, here we delivered TMS over DLPFC and examined its effect on the voxels located immediately under the coil.

Why did TMS not increase overall BOLD activity in the brain area under the coil in our study? This can be seen as puzzling given that TMS is known to induce action potential underneath the coil, which should then drive increased BOLD activity. There are a number of possible reasons. First, a number of studies demonstrated that TMS pulses can lead to an immediate increase

followed by a prolonged decrease in the firing rate of individual neurons in rats (Li et al., 2017), cats (Moliadze et al., 2003; Kozyrev et al., 2014), and monkeys (Grigsby, 2015; Romero et al., 2019b). These findings imply that, when integrated over an extended period of time, overall neural activity following a TMS pulse may not actually show an overall increase. Given the slow nature of the BOLD signal (Jezzard et al., 2001; Faro and Mohamed, 2006), it is likely that the observed activity in fMRI studies reflects the overall neural firing over an extended period of time rather than just the initial burst of firing, and therefore these animal studies could explain the lack of change in the BOLD signal observed here. Second, TMS may preferentially affect the white matter tracts that leave an area, rather than the cell bodies in that area. If so, one may expect that the TMS effects should be seen in downstream areas of the brain but not locally under the TMS coil. Finally, TMS may have additional effects other than making some neurons fire, and those effects may contribute to the BOLD response. For example, recent studies have suggested that TMS can directly inhibit cortical dendrites (Murphy et al., 2016). Note that these possibilities are not mutually exclusive and several of these processes may contribute to the fact that TMS does not produce reliable activations underneath the coil. Testing these possibilities requires animal studies where BOLD activity is measured while neurons are artificially stimulated. Beyond revealing more about the mechanisms of TMS, such studies can shed further light on the nature and correlates of the BOLD signal itself.

Our results add important new evidence regarding the local effects of TMS under the coil outside the motor and visual cortices in the absence of a task. Previous research on this topic found inconsistent results with some studies reporting an increase of activity under the coil

(Nahas et al., 2001; Li et al., 2004a; Bestmann et al., 2005; Vink et al., 2018a), while many others reported no such increase (Baudewig et al., 2001; Kemna and Gembris, 2003; Li et al., 2004b; Sack et al., 2007; De Weijer et al., 2014; Hawco et al., 2017; Dowdle et al., 2018). Critically, none of the studies that reported increased activity "under the coil" in the absence of a task actually had a precise estimate of exactly where the coil was positioned or defined the area under the coil as a region of interest. Instead, these studies typically reported any activations in a relatively large anatomical area that was in the rough vicinity of the TMS coil as being "under the coil." This is especially problematic because TMS induces both sensory (auditory and tactile) stimulation and corresponding cognitive processes, making it unsurprising that activation somewhere in the rough vicinity of the coil would be observed even if TMS did not increase or decrease activity immediately underneath the coil. In fact, by analyzing a large enough area around where the TMS coil is positioned, it would be easy to simultaneously find both an increase and a decrease "under the coil." By precisely localizing the actual location of stimulation and conducting ROI analyses, we were able to examine the effects of TMS immediately underneath the coil rather that searching a large area of cortex.

It could be argued that the differences between the studies that found activations under the TMS coil and studies that did not find such activations are due to differences in stimulation intensities, frequencies, number of pulses, or sites of stimulation. For example, it is possible that some sites of stimulation (e.g., premotor cortex) behave differently from others (e.g., DLPFC) or that activations under the coil would only be observed for specific intensities or frequencies. Nevertheless, many of the studies that reported activation under the coil used

lower intensities and lower frequencies than other studies that found no activations under the coil in roughly the same brain regions. Therefore, we contend that the discrepancies in the literature are likely due to the differences in analysis techniques highlighted above and not to the variability in stimulation parameters and locations.

It should be noted, however, that our conclusions apply exclusively to the effects of TMS in the absence of a task. It is quite possible that when TMS is delivered during a task that recruits a specific brain region, TMS would have an overall univariate effect on the BOLD activity in that region. Indeed, some previous studies have used an ROI approach and found that TMS changed the activity under the coil in the presence of a task (Feredoes et al., 2011; Heinen et al., 2014b) even though at least one of them suggested that the same stimulation parameters had no effect in the absence of a task (Heinen et al., 2014b).

Our results showed that even though TMS did not affect the univariate BOLD activity under the coil, the TMS different conditions could be reliably decoded using MVPA in both of our experiments. Furthermore, we found that the most informative voxels for classification were located near the surface of the brain where the stimulation strength is the highest. These findings suggest that TMS does influence BOLD activity even in the absence of a task but that the TMS effects may differ even for nearby neuronal populations thus producing a complex pattern of activations and deactivations that can be detected using MVPA but not with standard univariate techniques.

Finally, we note several limitations in our experiments. First, both of our experiments had only a few subjects. However, we collected large amount of data for each subject and performed the analyses at the individual level. This strategy was necessitated by the variability in the actual stimulation site between subjects, which does not allow for aggregation across subjects. Given that we observed similar results across our five subjects in Experiment 1 and all 12 individual sessions in Experiment 2, it is unlikely that larger samples would lead to different conclusions. In addition, we collected two different TMS sessions in Experiment 2 in order to increase the power to detect effects at the individual level. However, despite the use of neuronavigation, the actual site of stimulation differed slightly between the two sessions, making it impossible to pool the data across the two sessions as the region immediately underneath the coil had shifted. Therefore, to avoid such issues, we suggest that future concurrent TMS-fMRI experiments employ a single TMS session.

In conclusion, we found that, across two different experiments, TMS intensity and frequency could be decoded using MVPA even though TMS did not increase BOLD activity under the coil. These findings help settle a longstanding discrepancy in the literature and provide important insight into the mechanisms through which TMS influences neural activity.

References

Bang JW, Milton D, Sasaki Y, Watanabe T, Rahnev D (2019) Post-training TMS abolishes performance improvement and releases future learning from interference. Commun Biol 2:1–7 Available at: http://dx.doi.org/10.1038/s42003-019-0566-4.

Baudewig J, Frahm J, Tergau F, Tings T, Paulus W, Siebner HR, Bestmann S (2001) Functional MRI of cortical activations induced by transcranial magnetic stimulation (TMS). Neuroreport 12:3543–3548.

Bergmann TO, Karabanov A, Hartwigsen G, Thielscher A, Siebner HR (2016) Combining non-invasive transcranial brain stimulation with neuroimaging and electrophysiology: Current approaches and future perspectives. Neuroimage 140:4–19.

Bestmann S, Baudewig J, Siebner HR, Rothwell JC, Frahm J (2003) Subthreshold high-frequency TMS of human primary motor cortex modulates interconnected frontal motor areas as detected by interleaved fMRI-TMS. Neuroimage 20:1685–1696.

Bestmann S, Baudewig J, Siebner HR, Rothwell JC, Frahm J (2004) Functional MRI of the immediate impact of transcranial magnetic stimulation on cortical and subcortical motor circuits. Eur J Neurosci 19:1950–1962.

Bestmann S, Baudewig J, Siebner HR, Rothwell JC, Frahm J (2005) BOLD MRI responses to repetitive TMS over human dorsal premotor cortex. Neuroimage 28:22–29.

Bestmann S, Feredoes E (2013) Combined neurostimulation and neuroimaging in cognitive neuroscience: Past, present, and future. Ann N Y Acad Sci.

Bestmann S, Oliviero A, Voss M, Dechent P, Lopez-Dolado E, Driver J, Baudewig J (2006) Cortical correlates of TMS-induced phantom hand movements revealed with concurrent TMS-

fMRI. Neuropsychologia 44:2959–2971.

Bestmann S, Ruff CC, Blankenburg F, Weiskopf N, Driver J, Rothwell JC (2008) Mapping causal interregional influences with concurrent TMS–fMRI. Exp Brain Res 191:383–402.

Boecker H, Kleinschmidt A, Requardt M, Hanicke W, Merboldt KD, Frahm J (1994) Functional cooperativity of human cortical motor areas during self-paced simple finger movements a high-resolution MRI study. Brain.

Bohning DE, Pecheny AP, Epstein CM, Speer AM, Vincent DJ, Dannels W, Georgie MS (1997) Mapping transcranial magnetic stimulation (TMS) fields in vivo with MRI. 8:2535–2538.

Bohning DE, Shastri A, McConnell KA, Nahas Z, Lorberbaum JP, Roberts DR, Teneback C, Vincent DJ, George MS (1999) A combined TMS/fMRI study of intensity-dependent TMS over motor cortex. Biol Psychiatry.

Bohning DE, Shastri A, McGavin L, McConnell KA, Nahas Z, Lorberbaum JP, Roberts DR, George MS (2000a) Motor cortex brain activity induced by 1-Hz transcranial magnetic stimulation is similar in location and level to that for volitional movement. Invest Radiol.

Bohning DE, Shastri A, Wassermann EM, Ziemann U, Lorberbaum JP, Nahas Z, Lomarev MP, George MS (2000b) Bold-fMRI response to single-pulse transcranial magnetic stimulation (TMS). J Magn Reson Imaging.

Brett M, Anton J-L, Valabregue R, Poline J-B (2002) Region of interest analysis using an SPM toolbox. Neuroimage 16:S497.

Caparelli EC, Backus W, Telang F, Wang G-J, Maloney T, Goldstein RZ, Anschel D, Henn F (2010) Simultaneous TMS-fMRI of the Visual Cortex Reveals Functional Network, Even in Absence of Phosphene Sensation. Open Neuroimag J 4:100–110.

De Weijer AD, Sommer IEC, Bakker EJ, Bloemendaal M, Bakker CJG, Klomp DWJ, Bestmann S, Neggers SFW (2014) A setup for administering TMStoMedialand lateralcortical areas during whole-brain fMRI recording. J Clin Neurophysiol 31:474–487.

Dechent P, Frahm J (2003) Functional somatotopy of finger representations in human primary motor cortex. Hum Brain Mapp.

Denslow S, Bohning DE, Bohning PA, Lomarev MP, George MS (2005a) An increased precision comparison of TMS-induced motor cortex BOLD fMRI response for image-guided versus function-guided coil placement. Cogn Behav Neurol 18:119–126.

Denslow S, Lomarev M, George MS, Bohning DE (2005b) Cortical and subcortical brain effects of Transcranial Magnetic Stimulation (TMS)-induced movement: An interleaved TMS/functional magnetic resonance imaging study. Biol Psychiatry 57:752–760.

Dowdle LT, Brown TR, George MS, Hanlon CA (2018) Single pulse TMS to the DLPFC, compared to a matched sham control, induces a direct, causal increase in caudate, cingulate, and thalamic BOLD signal. Brain Stimul 11:789–796 Available at: https://doi.org/10.1016/j.brs.2018.02.014.

Faro SH, Mohamed FB (2006) Functional MRI: basic principles and clinical applications. Springer Science & Business Media.

Feredoes E, Heinen K, Weiskopf N, Ruff C, Driver J (2011) Causal evidence for frontal involvement in memory target maintenance by posterior brain areas during distracter interference of visual working memory. Proc Natl Acad Sci 108:17510–17515.

Frank E, Hall MA, Witten IH (2016) The WEKA Workbench. Online Appendix for “Data Mining: Practical Machine Learning Tools and Techniques.” Morgan Kaufmann:128 Available at:

http://www.cs.waikato.ac.nz/ml/weka/Witten_et_al_2016_appendix.pdf.

Grigsby EM (2015) The effects of transcranial magnetic stimulation (TMS) on the neural activity of awake non-human primates. Available at: https://hdl.handle.net/10161/9990.

Hawco C, Armony JL, Daskalakis ZJ, Berlim MT, Chakravarty MM, Pike GB, Lepage M (2017) Differing Time of Onset of Concurrent TMS-fMRI during Associative Memory Encoding: A Measure of Dynamic Connectivity. Front Hum Neurosci.

Hawco C, Voineskos AN, Steeves JKE, Dickie EW, Viviano JD, Downar J, Blumberger DM, Daskalakis ZJ (2018) Spread of activity following TMS is related to intrinsic resting connectivity to the salience network: A concurrent TMS-fMRI study. Cortex 108:160–172 Available at: https://doi.org/10.1016/j.cortex.2018.07.010.

Hebart MN, Görgen K, Haynes JD (2015) The decoding toolbox (TDT): A versatile software package for multivariate analyses of functional imaging data. Front Neuroinform 8:1–18.

Heinen K, Feredoes E, Weiskopf N, Ruff CC, Driver J (2014a) Direct evidence for attention-dependent influences of the frontal eye-fields on feature-responsive visual cortex. Cereb Cortex 24:2815–2821.

Heinen K, Feredoes E, Weiskopf N, Ruff CC, Driver J (2014b) Direct evidence for attention-dependent influences of the frontal eye-fields on feature-responsive visual cortex. Cereb Cortex.

Huth AG, De Heer WA, Griffiths TL, Theunissen FE, Gallant JL (2016) Natural speech reveals the semantic maps that tile human cerebral cortex. Nature 532:453–458.

Jezzard P, Matthews PM, Smith SM (2001) Functional MRI: An Introduction to Methods. Oxford: Oxford university press.

Kemna LJ, Gembris D (2003) Repetitive transcranial magnetic stimulation induces different responses in different cortical areas: A functional magnetic resonance study in humans. Neurosci Lett.

Kozyrev V, Eysel UT, Jancke D (2014) Voltage-sensitive dye imaging of transcranial magnetic stimulation-induced intracortical dynamics. Proc Natl Acad Sci U S A 111:13553–13558.

Langs G, Menze BH, Lashkari D, Golland P (2011) Detecting stable distributed patterns of brain activation using Gini contrast. Neuroimage.

Leitão J, Thielscher A, Tünnerhoff J, Noppeney U (2015) Concurrent TMS-fMRI reveals interactions between dorsal and ventral attentional systems. J Neurosci 35:11445–11457.

Li B, Virtanen JP, Oeltermann A, Schwarz C, Giese MA, Ziemann U, Benali A (2017) Lifting the veil on the dynamics of neuronal activities evoked by transcranial magnetic stimulation. Elife 6:1–22.

Li X, Nahas Z, Kozel FA, Anderson B, Bohning DE, George MS (2004a) Acute left prefrontal transcranial magnetic stimulation in depressed patients is associated with immediately increased activity in prefrontal cortical as well as subcortical regions. Biol Psychiatry.

Li X, Tenebäek CC, Nahas Z, Kozel FA, Large C, Cohn J, Bohning DE, George MS (2004b) Interleaved transcranial magnetic stimulation/functional MRI confirms that lamotrigine inhibits cortical excitability in healthy young men. Neuropsychopharmacology 29:1395–1407.

Moliadze V, Zhao Y, Eysel U, Funke K (2003) Effect of transcranial magnetic stimulation on single-unit activity in the cat primary visual cortex. J Physiol 553:665–679.

Murphy SC, Palmer LM, Nyffeler T, Müri RM, Larkum ME (2016) Transcranial magnetic

stimulation (TMS) inhibits cortical dendrites. Elife 5:1–12.

Nahas Z, Lomarev M, Roberts DR, Shastri A, Lorberbaum JP, Teneback C, McConnell K, Vincent DJ, Li X, George MS, Bohning DE (2001) Unilateral left prefrontal transcranial magnetic stimulation (TMS) produces intensity-dependent bilateral effects as measured by interleaved BOLD fMRI. Biol Psychiatry.

Navarro de Lara LI, Tik M, Woletz M, Frass-Kriegl R, Moser E, Laistler E, Windischberger C (2017a) High-sensitivity TMS/fMRI of the Human Motor Cortex Using a Dedicated Multichannel MR Coil. Neuroimage 150:262–269 Available at: http://dx.doi.org/10.1016/j.neuroimage.2017.02.062.

Navarro de Lara LI, Tik M, Woletz M, Frass-Kriegl R, Moser E, Laistler E, Windischberger C (2017b) High-sensitivity TMS/fMRI of the Human Motor Cortex Using a Dedicated Multichannel MR Coil. Neuroimage 150:262–269 Available at: http://dx.doi.org/10.1016/j.neuroimage.2017.02.062.

Navarro De Lara LI, Windischberger C, Kuehne A, Woletz M, Sieg J, Bestmann S, Weiskopf N, Strasser B, Moser E, Laistler E (2015) A novel coil array for combined TMS/fMRI experiments at 3 T. Magn Reson Med 74:1492–1501.

Pasley BN, Allen EA, Freeman RD (2009) State-Dependent Variability of Neuronal Responses to Transcranial Magnetic Stimulation of the Visual Cortex. Neuron 62:291–303.

Pinheiro J, Bates D, DebRoy S, Sarkar D, Maintainer R (2019) package “nlme”: Linear and Nonlinear Mixed Effects Models. Available at: https://cran.r-project.org/package=nlme.

Polanía R, Nitsche MA, Ruff CC (2018) Studying and modifying brain function with non-invasive brain stimulation. Nat Neurosci 21:174–187.

Rahnev D, Kok P, Munneke M, Bahdo L, de Lange FP, Lau H (2013) Continuous theta burst transcranial magnetic stimulation reduces resting state connectivity between visual areas. J Neurophysiol 110:1811–1821 Available at: https://www.physiology.org/doi/10.1152/jn.00209.2013 [Accessed March 6, 2020].

Rahnev D, Nee DE, Riddle J, Larson AS, D'Esposito M (2016) Causal evidence for frontal cortex organization for perceptual decision making. Proc Natl Acad Sci 113:6059–6064.

Romero MC, Davare M, Armendariz M, Janssen P (2019a) Neural effects of transcranial magnetic stimulation at the single-cell level. Nat Commun 10:1–11.

Romero MC, Davare M, Armendariz M, Janssen P (2019b) Neural effects of transcranial magnetic stimulation at the single-cell level. Nat Commun 10:1–11 Available at: http://dx.doi.org/10.1038/s41467-019-10638-7.

Ruff CC, Driver J, Bestmann S (2009) Combining TMS and fMRI: From "virtual lesions" to functional-network accounts of cognition. Cortex 45:1043–1049 Available at: http://dx.doi.org/10.1016/j.cortex.2008.10.012.

Sack AT, Kohler A, Bestmann S, Linden DEJ, Dechent P, Goebel R, Baudewig J (2007) Imaging the brain activity changes underlying impaired visuospatial judgments: Simultaneous fMRI, TMS, and behavioral studies. Cereb Cortex 17:2841–2852.

Shekhar M, Rahnev D (2018) Distinguishing the roles of dorsolateral and anterior PFC in visual metacognition. J Neurosci 38:5078–5087.

Triantafyllou C, Polimeni JR, Wald LL (2011) Physiological noise and signal-to-noise ratio in fMRI with multi-channel array coils. Neuroimage 55:597–606 Available at: http://dx.doi.org/10.1016/j.neuroimage.2010.11.084.

Vink JJT, Mandija S, Petrov PI, van den Berg CAT, Sommer IEC, Neggers SFW (2018a) A novel concurrent TMS-fMRI method to reveal propagation patterns of prefrontal magnetic brain stimulation. Hum Brain Mapp 39:4580–4592.

Vink JJT, Mandija S, Petrov PI, van den Berg CAT, Sommer IEC, Neggers SFW (2018b) A novel concurrent TMS-fMRI method to reveal propagation patterns of prefrontal magnetic brain stimulation. Hum Brain Mapp.

Wang WT, Xu B, Butman JA (2017) Improved SNR for combined TMS-fMRI: A support device for commercially available body array coil. J Neurosci Methods 289:1–7 Available at: http://dx.doi.org/10.1016/j.jneumeth.2017.06.020.

Supplementary Materials

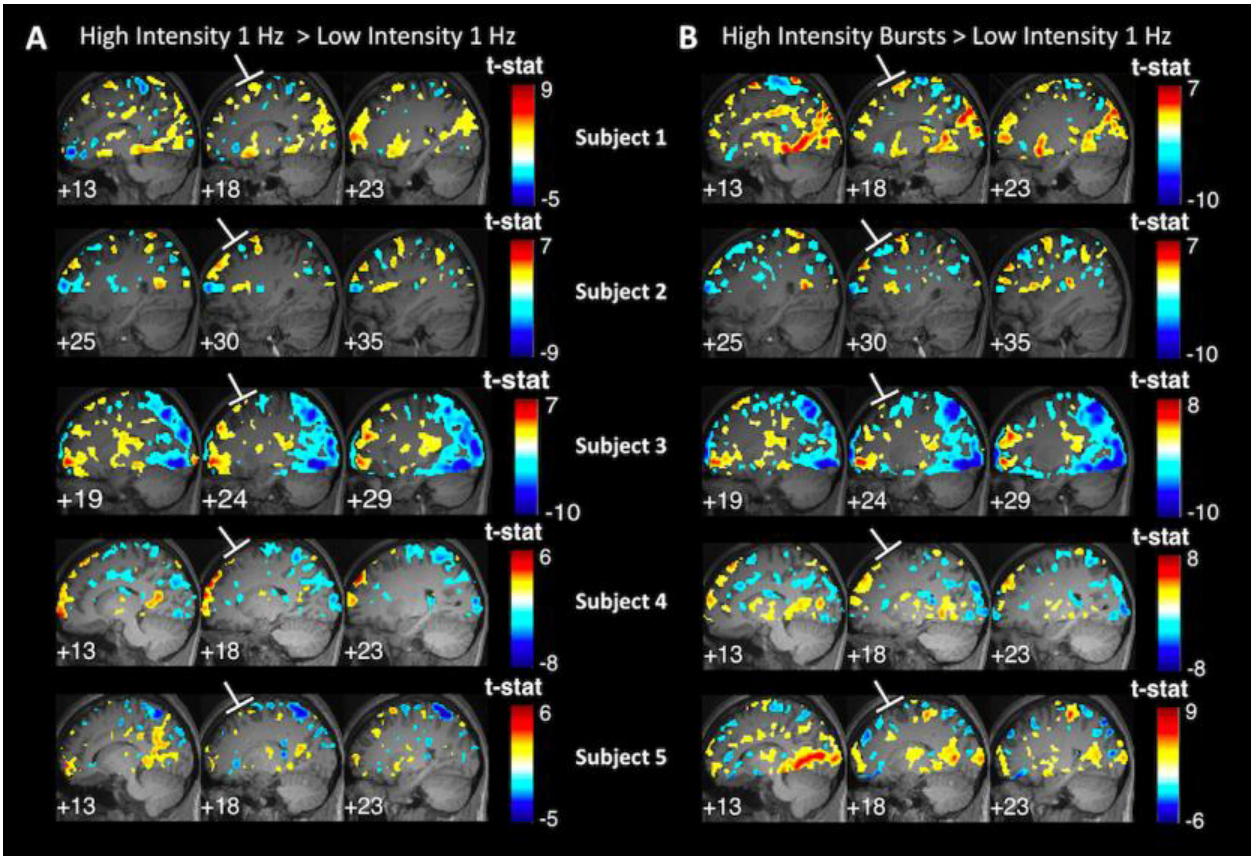

Supplementary Figure 1. TMS to DLPFC produces no activation under the coil even at *p* < .05, uncorrected. We contrasted each of the two high-intensity TMS conditions against the low-intensity TMS condition, but, unlike in Figure 3, used an even more liberal threshold for significance (*p* < .05, uncorrected). (A) High intensity 1 Hz > Low intensity 1 Hz contrast. (B) High intensity bursts > Low intensity 1 Hz contrast. For both panels, sagittal slices are centered at the site of stimulation (middle column) and 5 mm to the left and right. The activation maps show a lack of systematic activation immediately under the coil and suggest the presence of large variability in remote areas across subjects. Colors indicate t-values.